

Self-Assembly of Asymmetrically Interacting ABC Star Triblock Copolymer Melts

Kai Jiang,^{*} Juan Zhang,^{*} and Qin Liang

*Hunan Key Laboratory for Computation and Simulation in Science and Engineering, School of
Mathematics and Computational Science (Xiangtan University), Hunan 411105, China*

E-mail: kaijiang@xtu.edu.cn; zhangjuan@xtu.edu.cn

Abstract

The phase behavior of asymmetrically interacting ABC star triblock copolymer melts is investigated by the self-consistent field theory (SCFT). Motivated by the experimental systems, in this study, we focus on the systems in which the Flory-Huggins interaction parameters satisfy $\chi_{AC} > \chi_{BC} \approx \chi_{AB}$. Using various initialization strategies, a large number of periodic structures have been obtained in our calculations. A fourth-order pseudospectral algorithm combined with Anderson mixing method is used to compute the free energy of candidate structures carefully. The stability has been detailedly analyzed by splitting the free energy into internal and entropic parts. A complete and complex triangular phase diagram is presented for a model with $\chi_{AC} > \chi_{BC} = \chi_{AB}$ in which fifteen ordered phases, including two-, and three-dimensional structures, have been predicted to be stable from the SCFT calculations. Generally speaking, with the asymmetrical interactions, the hierarchical structures tend to be formed near the B-rich corner of the triangular phase diagram. This work broadens the previous theoretical results from equal interaction systems to unequal interaction systems. The predicted phase behavior is in good agreement with experimental observations and previous theoretical results.

^{*}To whom correspondence should be addressed

Introduction

Block copolymers, constructed by linking together chemically distinct subchains or blocks, spontaneously assemble into exquisitely ordered soft materials.^{1,2} The self-assembled order structures, spanning length scales from a few nanometers to several micrometers, offer a diverse and expanding range of practical applications in, for example, optical materials, microelectronic materials, drug delivery, advanced plastics, and nanotemplates.³⁻⁵

The development of nanotechnology using block copolymers requires a good understanding of the phase behavior of the block copolymers. The self-assembling mechanism of block copolymers sensitively depends on block types, the number of blocks, block-block interactions, architecture, and topology of the block polymers. The equilibrium ordered patterns can be formed due to the delicate balance between these competing factors. In ABC triblock copolymers, the number of controlled parameters is at least five, including three interaction parameters $\chi_{AB}N$, $\chi_{AC}N$, $\chi_{BC}N$, and two independent block compositions f_A and f_B . N is the degree of polymerization and $\chi_{\alpha\beta}$ is the Flory-Huggins interaction parameter characterizing the interaction between two chemically different blocks α and β . Compared with linear copolymers, the star-shaped copolymers have complicated phase behavior or physical properties induced by different molecular architecture. In the ordered phases of ABC star triblock copolymers, the most distinct feature is the arrangement of the junction points. If the chain lengths of three blocks are comparable, junction points are aligned on a one-dimensional (1D) straight line, then cylindrical morphologies can be formed naturally. Their cross sections tend to show two-dimensional (2D) patterns since polymer/polymer interfaces can be flat surfaces due to the repulsion forces between “unconnected” branches. These factors lead to the formation of 2D polygonal tiling patterns, or Archimedean tiling. The tiling patterns can be encoded by a set of integers $[k, l, m, \dots]$, indicating that a k -gon, an l -gon, and an m -gon, etc., meet consecutively at each vertex. If some asymmetry, to the contrary, is introduced to the compositions, the junction points are mostly aligned on the curved trails. Consequently three-dimensional (3D) structures can be formed. Furthermore, when the interactions are strong enough, the ABC star triblock copolymers can self-assemble into hierarchical structures.^{6,7}

Owing to the rich phase behavior, a number of experiments have been carried out on the phase and phase transition of ABC star triblock copolymers in past decades.^{6–18} In particular, Matsushita and co-workers have conducted systematic studies on the morphologies formation of (polyisoprene-polystyrene-poly(2-vinylpyridine)) (ISP) star triblock copolymers. Several ordered tiling patterns, such as [6.6.6], [8.8.4], [12.6.4], [3.3.4.3.4], and even a dodecagonal symmetric quasicrystalline tiling,¹⁹ have been observed in the ISP star triblock copolymers.^{6,7,11–14} Meanwhile, several hierarchical structures including cylinders-in-lamella, lamellae-in-cylinder, lamellae-in-sphere, and hierarchical double gyroid structures are also discovered with the asymmetries of composition.^{6,7,15} Recently, Nunns et al. used polyisoprene (I), polystyrene (S) and poly-(ferrocenylethylmethylsilane) (F) to synthesize ISF star triblock copolymers.¹⁷ Three 2D patterns, including [8.8.4], [12.6.4], and lamellae with alternating cylinders, were observed. Both of the experimental systems satisfy asymmetrical interaction between different blocks, i.e., $\chi_{AC}N > \chi_{BC}N \approx \chi_{AB}N$. In particular, in ISP star triblock copolymers, the interaction strengths are known to follow the order $\chi_{IS}N \approx \chi_{SP}N < \chi_{IP}N$,⁶ while in ISF star-shaped triblock copolymers, $\chi_{SF}N \approx \chi_{IS}N < \chi_{IF}N$.¹⁷

Besides experimental works, theoretical studies provide a good understanding of phase behavior of ABC star triblock copolymers. Bohbot-Raviv and Wang²⁰ used a coarse-grained free energy functional to numerically investigate some morphologies of ABC star triblock copolymers. In 2002, Gemma and co-workers²¹ carried out Monte Carlo (MC) simulations on ABC star triblock copolymers with equal interactions between the three components. The phase behavior of ABC star triblock copolymers with composition ratio of, $f_A : f_B : f_C = 1.0 : 1.0 : x$, was investigated in detail in strong segregation region. Five kinds of 2D cylindrical phases, three kinds of lamellar-type phases and two kinds of continuous matrix phases were obtained from the MC simulations. Huang and co-workers²² studied the effects of composition and interaction parameter on the phase behavior of ABC star copolymers with equal interactions among the three components using dissipative particle dynamics (DPD) simulations. Several efforts have also been made to study the phase behavior of ABC star triblock copolymers using the SCFT.^{23–27} In 2004, Tang

et al.²³ started to use a 2D SCFT simulation to study the phase behavior of ABC star triblock copolymers. Based on the SCFT, Zhang et al.²⁴ and Li et al.²⁵ examined the weak and intermediate segregation cases of mainly 2D structures with equal interactions. Zhang et al.²⁴ also chose $\chi_{AB}N = \chi_{BC}N = 25.0$, $\chi_{AC}N = 37.0$ to model the ISP star triblock copolymer system of the type $A_{1.0}B_{1.0}C_x$. Accordingly, a 1D phase diagram was obtained as a function of x from 0.5 to 2.0. The stability of the different lamellar morphologies formed from ABC star triblock copolymers has been examined by Xu et al.²⁶ These SCFT studies mainly focus on the symmetrically interacting systems and the phase behavior of 2D structures. Despite these previous experimental and theoretical studies, a comprehensive understanding of ABC star triblock copolymers is still lacking, especially for the asymmetric interaction systems. In this work, we will explore the phase behavior of ABC star triblock copolymers, including 2D and 3D structures, with asymmetric interaction parameters between chemically different blocks.

Theoretical approaches to investigating the phase behavior of block copolymers, often involve minimizing an appropriate free energy functional of the system, and comparing the free energies of different candidate structures. Therefore a systematic examination of the emergence and stability of ordered phases requires the availability of suitable free energy functionals and accurate methods to compute the free energy of ordered phases. Owing to a large number of studies, it has been well proven that the SCFT provides a powerful theoretical framework for the study of the phase behavior of block copolymers.^{28,29} In particular, the SCFT can be used to determine the relative stability of different phases because it provides an accurate estimate of the free energy. The essence of the SCFT is that the free energy of the system can be written as a functional of the spatially varying polymer densities and a set of conjugate fields. Minimizing the free energy functional with respect to the densities and conjugate fields leads to a set of equations, encoded as SCFT equations. The SCFT equations are a set of highly nonlinear equations with multi-solutions which correspond to the different ordered phases of block copolymers. The equations also have a strong nonlocality that emerges from the connection of propagators and densities, conjugate fields.

Solving the SCFT equations requires iterative techniques. Owing to the nature of iterative

methods, the solutions sensitively depend on the initial configuration at the start of the iteration. A series of efficient strategies of screening initial conditions are developed based on the fact that all periodic structures belong to one of 230 space groups.^{27,30,31} In each iterative step, efficient numerical schemes are required to solve the propagator equations. In the past years, two complementary methods, including spectral methods^{32,33} and real-space methods³⁴ to solve the SCFT equations have been developed. In recent years, an efficient pseudospectral method has been introduced to solve propagator equations.^{35–37} This algorithm takes advantage of the best features of real- and Fourier-space with the computational effort scale of $O(N \log N)$ based on the fast Fourier transformation (FFT). N is the number of spectral modes or discrete points in real-space. To obtain the solutions of the SCFT equations corresponding to the saddle points of the SCFT free energy functional, the iterative methods are required to make the iteration convergent. The quasi-Newton methods were employed in the fully spectral approach to the SCFT by Matsen and Schick.³² A simple mixing method by a linear combination of two consecutive fields was introduced by Drolet and Fredrickson³⁴ for the SCFT simulations. Recently the Anderson mixing method^{40,41} has been proven by itself to greatly reduce the number of SCFT iterations. From the perspective of nonlinear optimization, Cenicerros and Fredrickson³⁸ devised a class of efficient semi-implicit schemes for solving the SCFT equations using the asymptotic expansion technology. Later, Jiang et al.³⁹ have extended these algorithms to the SCFT calculations for multicomponent polymer systems.

A generic strategy of theoretical studying phase behavior of complex block copolymer systems includes two steps.^{25,27} The first step involves an efficient strategy to produce a library of possible candidate structures. In the second step, the candidate structures are used as initial conditions in the more accurate methods to compute free energies, which are used to construct phase diagrams of the systems. In this work, we apply this strategy to examine the phase behavior of ABC star triblock copolymers using the SCFT. Specifically, the strategies developed in our previous work²⁷ are used as a screening technique to obtain candidate structures as many as possible. These strategies include (1) knowledge from previous experiments and theories; (2) knowledge from related systems, for example, diblock copolymers; (3) combination and interpolation of known structures; and (4)

random initial configurations. Using these candidate structures as initial conditions, a fourth-order pseudospectral method combined with Anderson mixing method is employed to study the stability of ordered phases. To model the asymmetric interacting experimental systems of ISP and ISF, the interaction parameters of $\chi_{AC}N > \chi_{BC}N = \chi_{AB}N$ are used in our study. It should be emphasized that, to broaden the scope of the research, the 2D and 3D ordered phases are included in our calculations. The resulting free energies of the different ordered phases are used to construct phase diagrams.

Theory and Methods

We consider an incompressible melt of n ABC star triblock copolymers with a degree of polymerization N in a finite volume of V . The chain lengths, or compositions, of A, B, and C blocks are $f_A N$, $f_B N$, and $f_C N$ ($f_A + f_B + f_C = 1$), respectively. A characteristic length of the copolymer chain can be defined by the radius of gyration, which is used as the unit of length, so that all spatial lengths are presented in units of R_g . Within the mean-field approximation to statistical mechanics of the Edwards model of polymers, at a temperature T , the free energy functional F per chain of the Gaussian triblock copolymer melt is

$$\frac{F}{nk_B T} = -\log Q + \frac{1}{V} \int d\mathbf{r} \left\{ \sum_{\alpha \neq \beta} \chi_{\alpha\beta} N \phi_\alpha(\mathbf{r}) \phi_\beta(\mathbf{r}) - \sum_{\alpha} w_\alpha(\mathbf{r}) \phi_\alpha(\mathbf{r}) - \eta(\mathbf{r}) [1 - \sum_{\alpha} \phi_\alpha(\mathbf{r})] \right\}, \quad (1)$$

where $\alpha, \beta \in \{A, B, C\}$ are the block labels, ϕ_α is the monomer density of the α -blocks, and Q is the partition function of one star block copolymer chain in the mean field, $w_\alpha(\mathbf{r})$, produced by the surrounding chains. $\eta(\mathbf{r})$ is the Lagrange field to ensure the local incompressibility. The interactions between the three chemically distinct monomers are characterized by three Flory-Huggins interaction parameters multiplied by polymerization degree, i.e., $\chi_{BC}N$, $\chi_{AC}N$, and $\chi_{AB}N$. First-order variations of the free-energy functional with respect to the monomer densities and the conjugate

fields subjected to the incompressible condition lead to the following set of SCFT equations

$$w_A(\mathbf{r}) = \chi_{AB}N\phi_B(\mathbf{r}) + \chi_{AC}N\phi_C(\mathbf{r}) + \eta(\mathbf{r}), \quad (2)$$

$$w_B(\mathbf{r}) = \chi_{AB}N\phi_A(\mathbf{r}) + \chi_{BC}N\phi_C(\mathbf{r}) + \eta(\mathbf{r}), \quad (3)$$

$$w_C(\mathbf{r}) = \chi_{AC}N\phi_A(\mathbf{r}) + \chi_{BC}N\phi_B(\mathbf{r}) + \eta(\mathbf{r}), \quad (4)$$

$$1 = \phi_A(\mathbf{r}) + \phi_B(\mathbf{r}) + \phi_C(\mathbf{r}), \quad (5)$$

$$\phi_A(\mathbf{r}) = \frac{1}{Q} \int_0^{f_A} ds q_A(\mathbf{r}, s) q_A^\dagger(\mathbf{r}, f_A - s), \quad (6)$$

$$\phi_B(\mathbf{r}) = \frac{1}{Q} \int_0^{f_B} ds q_B(\mathbf{r}, s) q_B^\dagger(\mathbf{r}, f_B - s), \quad (7)$$

$$\phi_C(\mathbf{r}) = \frac{1}{Q} \int_0^{f_C} ds q_C(\mathbf{r}, s) q_C^\dagger(\mathbf{r}, f_C - s), \quad (8)$$

$$Q = \frac{1}{V} \int d\mathbf{r} q_K(\mathbf{r}, s) q_K^\dagger(\mathbf{r}, f_K - s), \quad \forall s, K. \quad (9)$$

In these expressions, the functions $q_K(\mathbf{r}, s)$ and $q_K^\dagger(\mathbf{r}, s)$ ($K \in \{A, B, C\}$) are the end-integrated segment distribution functions, or propagators, representing the probability of finding the s -th segment at a spatial position \mathbf{r} . These propagators satisfy the modified diffusion equations (MDEs)

$$\begin{aligned} \frac{\partial}{\partial s} q_K(\mathbf{r}, s) &= \nabla_{\mathbf{r}}^2 q_K(\mathbf{r}, s) - w_K q_K(\mathbf{r}, s), \quad q_K(\mathbf{r}, 0) = 1, \quad s \in [0, f_K], \\ \frac{\partial}{\partial s} q_K^\dagger(\mathbf{r}, s) &= \nabla_{\mathbf{r}}^2 q_K^\dagger(\mathbf{r}, s) - w_K q_K^\dagger(\mathbf{r}, s), \quad q_K^\dagger(\mathbf{r}, 0) = q_L(\mathbf{r}, f_L) q_M(\mathbf{r}, f_M), \end{aligned} \quad (10)$$

where $(KLM) \in \{(ABC), (BCA), (CAB)\}$. Numerically solving these SCFT equations involves an iterative procedure starting with an initial configuration of the fields $w_K(\mathbf{r})$ with $K \in A, B, C$. The MDEs (Eqn. (10)) are then solved to obtain the propagators, which are used to compute the densities $\phi_K(\mathbf{r})$ and to update the mean fields $w_K(\mathbf{r})$. The iteration is continued until these mean fields and densities are self-consistent such that they satisfy the SCFT equations within a prescribed numerical accuracy.

There are two main steps in studying the phase behavior of block copolymers. The first step is to obtain possible candidate structures as many as possible. Several strategies of exploring or-

dered phases have been proposed in our previous works.^{27,30} Beyond the random initial values, these approaches include (1) knowledge from experiments and theories, such as small-angle X-ray scattering images, space group theory for periodic structures; (2) knowledge from related systems; (3) combination and interpolation of known structures. Using these diverse strategies of initialization, a large number of ordered phases can be generated as the solutions of the SCFT equations. In addition, the possible candidate structures from previous theoretical and experimental studies are considered in our calculations. The second step is to identify the stability of these phases by comparing their free energies using efficient numerical methods. In this work, we combine an improved pseudospectral method with Anderson mixing algorithm to solve the SCFT equations for periodic block-copolymer morphologies. A fourth-order accurate Adams-Bashford scheme³⁶ is used to discretize the MDEs. The initial values required to apply this formula are obtained using a special extrapolation method,³⁷ based on the second-order operator-splitting scheme.³⁵ A modified integral formula for closed interval is chosen to solve the integrated equations (??)-(??) that can guarantee fourth-order precision in s -direction whether the number of discretization points is even or odd.⁴² To ensure the accuracy, we require that these substeps of contour length s are smaller than 0.01 in the fourth-order accurate scheme. The FFT is used to translate the data between real- and Fourier-space in the pseudospectral method.

To obtain the equilibrium morphologies of SCFT equations, iterative methods shall be required to update the conjugate fields. For this step we choose the Anderson mixing algorithm, firstly proposed by Anderson,⁴³ then introduced into polymer theoretical calculations by Schmid and Müller,⁴⁰ Thompson et al.⁴¹ Owing to the local convergence of this method, we use the simple mixing method alone at the start of the algorithm to obtain better initial values for the fields, followed by Anderson mixing approach alone to accelerate the convergent procedure to the prescribed accuracy in the fields. The Anderson mixing method requires the fields of previous n steps when update new fields. Using the previous n step fields, the Anderson mixing method produces an n -order linear equations system from a least square problem. Then the new fields will be obtained by a combination of the fields of previous n steps, with the solution of linear system being the

weight factors. For relatively simpler systems, such as diblock copolymers, the Anderson mixing algorithm can significantly reduce the required number of iterations with few histories.^{41,44} For more complex situation, a larger n shall be taken to update fields to accelerate the convergent procedure. We find that assembling the n -order linear system spends more computation time than solving this linear system. When n becomes too large, it will slow the iteration. Here we overcome this problem by rearranging the elements of the $n \times n$ matrix. The technical details can be found in the Appendix section. By using our approach, the Anderson mixing method can robustly converge without slowing the SCFT iterations. In practice, we use the available histories of 50 steps.

Here we only consider the periodic structures, therefore, periodic boundary conditions are imposed on each direction. In our calculations, all spatial functions are all expanded in terms of plane waves. For 2D morphologies, a square box is simulated. 128×128 plane-wave basis functions are used to discretize the 2D box. For 3D structures, we use a cubic unit cell in most of our calculations. The number of plane-wave basis functions is $32 \times 32 \times 32$. The size of computation box plays an important role in determining the stability of ordered phases. For a given phase, its free energy is minimized with respect to the box sizes by the steepest descent approach coupled with solving the SCFT equations.³⁰

Based on the discussion above, we summarize the iteration procedure by sketching the numerical recipes:

Step 1 Starting from the given initial conditions and computational box, the fourth-order pseudospectral method combined with Anderson mixing method is applied to obtain the ordered phases when the field's change is smaller than the prescribed error ε_1 .

Step 2 Optimizing the size of unit cell by minimizing the free energy with the steepest descent method.

Step 3 Goto **Step 1** until the free energy change is smaller than a given error ε_2 .

To ensure enough accuracy, in our implementation, each calculation is terminated until the field's change (defined in Appendix) at each iteration is reduced to $\varepsilon_1 = 10^{-6}$ (corresponding to a free

energy change of about 10^{-7}), and $\varepsilon_2 = 10^{-6}$. For the cases of $\chi_{AC}N = 50.0$, $\chi_{AB}N = \chi_{BC}N = 30.0$ in the current work, the relative values of free energy among different phases in determining the phase boundary are from $O(10^{-2})$ to $O(10^{-4})$. Therefore our numerical resolution is adequately accurate for constructing phase diagrams.

Results and Discussion

The previously theoretical studies mainly focus on the equally interacting ABC star triblock copolymer systems, i.e., $\chi_{BC}N = \chi_{AC}N = \chi_{AB}N$.^{21,22,24,25,27} However, under experimental circumstances as mentioned above, many ABC star triblock copolymers with asymmetric interactions have been synthesized to observe their phase behaviors, such as ISP⁶ and ISF¹⁷ star triblock copolymers. In particular, the interaction parameters of the above systems satisfy the relationship $\chi_{AB}N \approx \chi_{BC}N < \chi_{AC}N$. In order to make a meaningful comparison of the theoretical study and experimental investigation, the interaction parameters are chosen in the calculations so that they are appropriate for these experimental systems. Although accurate values of the Flory-Huggins parameters are not available in the literatures, qualitative interaction strengths are known to follow the order $\chi_{IS} \approx \chi_{SP} < \chi_{IP}$,^{6,12} $\chi_{SF} \approx \chi_{IS} < \chi_{IF}$.¹⁷ In what follows we choose asymmetric interaction parameters, $\chi_{AC}N = 50.0$, $\chi_{AB}N = \chi_{BC}N = 30.0$, and equal statistical segment lengths. This is a rough approximation to ISP and ISF copolymers, with the important difference that, in the idealized system, we neglect the small differences between $\chi_{AB}N$ and $\chi_{BC}N$.

As mentioned above, there are two main steps in studying the phase behavior of block copolymers. The first step is to obtain as many possible candidate structures as possible. The second step is to identify the stability of these patterns by comparing their free energies and construct the phase diagrams. In order to further analyse the stability of candidate patterns, it is helpful to split the free energy into two parts: internal (U) and entropic ($-TS$). The internal and entropic contributions to

the free energy can be expressed as²⁸

$$\begin{aligned}\frac{U}{nk_B T} &= \frac{1}{V} \int d\mathbf{r} \left\{ \sum_{\alpha \neq \beta} \chi_{\alpha\beta} N \phi_{\alpha}(\mathbf{r}) \phi_{\beta}(\mathbf{r}) \right\}, \\ -\frac{S}{nk_B T} &= -\log Q - \frac{1}{V} \int d\mathbf{r} \left\{ \sum_{\alpha} w_{\alpha}(\mathbf{r}) \phi_{\alpha}(\mathbf{r}) \right\},\end{aligned}\tag{11}$$

where $\alpha, \beta \in \{A, B, C\}$ are the block labels.

Candidate Patterns

Using different initialization procedures, a large number of candidate structures have been obtained in our previous work.²⁷ Here we only present the stable phases in the case of $\chi_{AC}N = 50.0$, $\chi_{AB}N = \chi_{BC}N = 30.0$, as shown in Fig. 1. Among these candidate phases, several polygon tiling patterns, or the cylindrical structures, with translation invariant along the third direction are found as 2D phases. These polygon patterns include [6.6.6], [8.8.4], [12.6.4], [3.3.4.3.4], [8.6.6;8.6.4], [10.6.6;10.6.4;8.6.6;8.6.4]. The first pattern is designated as [6.6.6] because each vertex in this tiling is surrounded by three hexagonal polygons. Similarly the second and third patterns are named [8.8.4] and [12.6.4], respectively. The fourth pattern looks more complex. There are two types of vertices: one is surrounded by 10-gon, 8-gon and 4-gon, whereas the other is formed by a decagon, a hexagon and a tetragon. From our naming convention, it should be named [10.8.4;10.6.4]. However, with the help of triangles and squares of hypothetical tiling, as Fig. 1 shows the superimposed tiling on a schematic drawing, it is noted all the meeting vertices are surrounded by three regular triangles and two squares, which is one of the Archimedean tilings. In order to compare with experimental results, we encode it as [3.3.4.3.4].¹² The fifth pattern also possesses two kinds of vertices: one is surrounded by 8-gon, 6-gon, and 4-gon, whereas the other is formed by an 8-gon and two 6-gons. Consequently, this pattern is designated as [8.6.4;8.6.6]. Similarly, the fifth pattern has four kinds of vertices, therefore, it is named [10.6.6;10.6.4;8.6.6;8.6.4]. Besides these polygonal phases, additional three 2D structures, i.e., three color lamellae (LAM), the core-shell cylinders (HC), and hierarchical cylinders-in-lamella phases (L+C) are also obtained

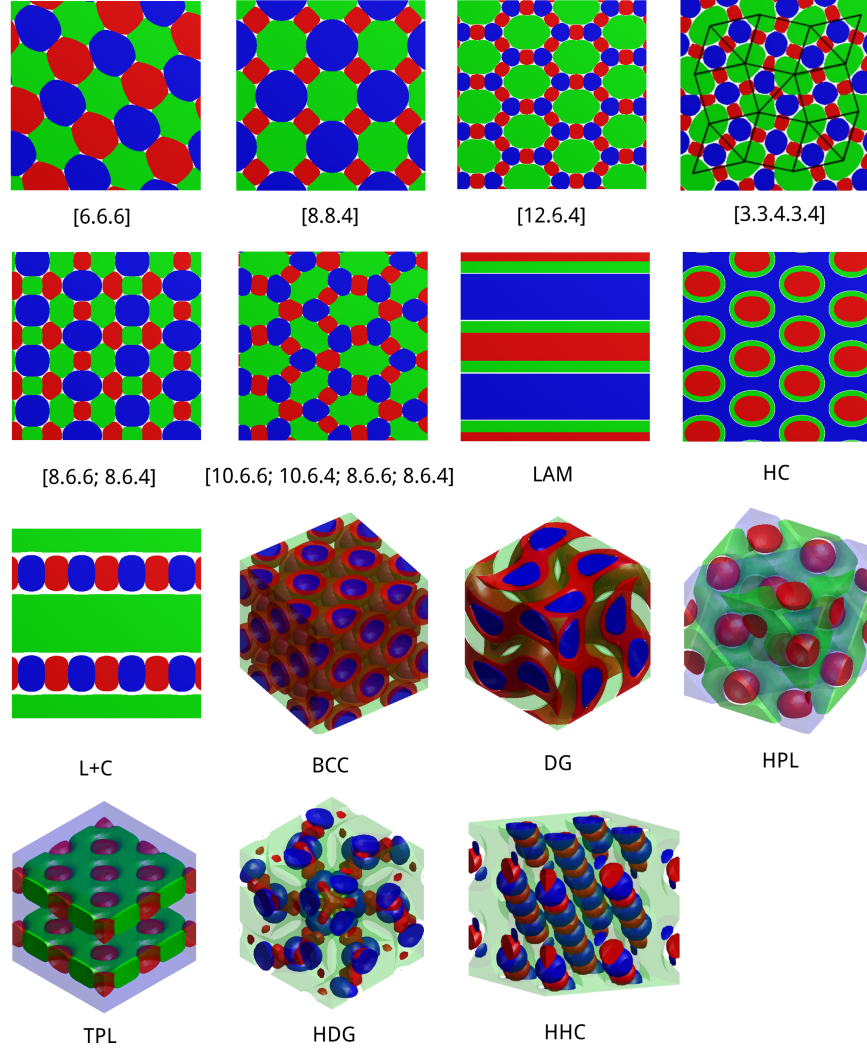


Figure 1: Ordered phases of ABC star triblock copolymers obtained using the SCFT calculations with $\chi_{AC}N = 50.0$, $\chi_{AB}N = \chi_{BC}N = 30.0$. The colors of red, green, and blue, indicate the regions where the most components are A, B, and C, respectively.

in our simulations. At the same time, a series of 3D structures are obtained. From the morphology of patterns, these 3D patterns can be classified into core-shell phases and hierarchical structures. The former includes core-shell spheres in body-centered-cubic lattice (BCC) and core-shell double-gyroid phases (DG). The hierarchical patterns consist of two kinds of hierarchical cylinders packed hexagonally (HHC), two kinds of cylinders-in-lamella phases, with the cylinders being packed hexagonally (HPL) and tetragonally (TPL), and hierarchical gyroid phases (HDG). Note that due to the equal interaction parameters of $\chi_{AB}N = \chi_{BC}N$, these structures have their mirror phases along the phase path of isopleth $f_A = f_C$.

Phase Behavior of $A_{1.0}B_{1.0}C_x$ Star Triblock Copolymers

In a series of experiments,^{12,13,17,46} two of the three arms are kept to be of equal length and the arm-length ratio is expressed as $1.0 : 1.0 : x$. Motivated by these experiments, we start with the calculation of the phase stability along this phase path. Here we assume that A and B arms have equal length and the C arm holds the arm-length ratio of $x = f_C/f_A$. The free energy differences of candidate phases from the value of the homogeneous phase as a function of the volume fraction of f_C are given in Fig. 2 (a). The phase stability regions as a function of x are presented in Fig. 2 (b). In Fig. 2 (a), the free energies of some metastable phases along this path are not shown, such as that of [10.6.6;10.6.4;8.6.6;8.6.4] in the region of $0.32 \leq f_C \leq 0.46$, where it has higher free energy than [6.6.6], or $[8.8.4]^2$, or [3.3.4.3.4]. With the increase of x , the phase sequence is $LAM^1 \rightarrow [8.8.4]^1 \rightarrow [8.6.6;8.6.4] \rightarrow [6.6.6] \rightarrow [8.8.4]^2 \rightarrow [3.3.4.3.4] \rightarrow [12.6.4] \rightarrow TPL \rightarrow LAM^2$. The corresponding stable regions are $x \leq 0.435$ (LAM^1), $0.435 \leq x \leq 0.67$ ($[8.8.4]^1$), $0.67 \leq x \leq 0.71$ ($[8.6.6;8.6.4]$), $0.71 \leq x \leq 1.04$ ($[6.6.6]$), $1.04 \leq x \leq 1.39$ ($[8.8.4]^2$), $1.39 \leq x \leq 1.68$ (3.3.4.3.4), $1.68 \leq x \leq 2.05$ ($[12.6.4]$), $2.05 \leq x \leq 2.76$ (TPL), and $x \geq 2.76$ (LAM^2), respectively. When f_C is small, in one period, the lamellar structure of LAM^1 of CACB type includes two thick A and B layers, and two thin C layers. The symbols of $[8.8.4]^1$ and $[8.8.4]^2$ are used to distinguish the 4-coordinated polygons segregated by different block. In the $[8.8.4]^1$ phase, the minority C-arms form the 4-coordinated domains, and blocks A and B alternatively form 8-coordinated

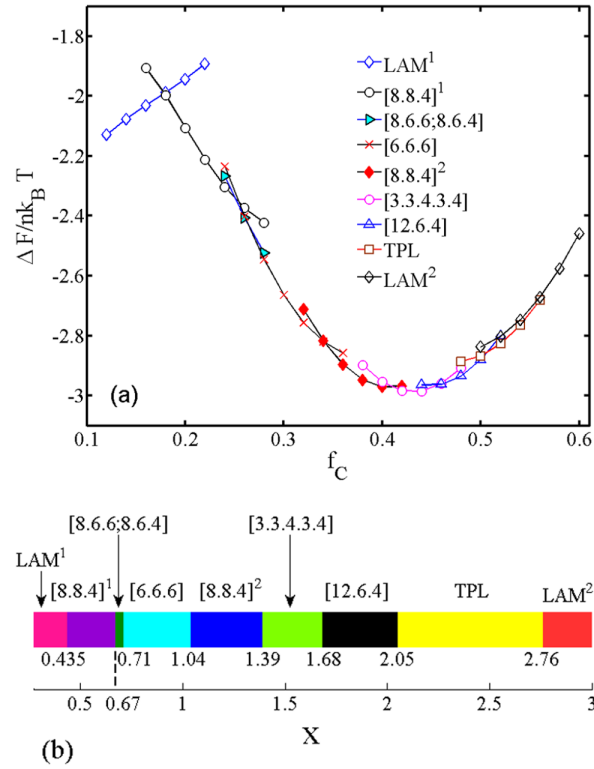


Figure 2: (a) Free energy differences from the value of the homogeneous phase as a function of the volume fraction of C composition for ABC star triblock copolymers with symmetric A and B arms. (b) Phase stability regions as a function of the arm-length ratio of $x = f_C/f_A$ ($f_A = f_B$). Note that in the $[8.8.4]^1$ phase, the minority C blocks form the 4-coordinated domains, and blocks A and B alternatively form 8-coordinated microdomains. While in the $[8.8.4]^2$ morphology, the A and C blocks form the 8-coordinated polygons, and B blocks form the domains with 4-coordinations. In one periodicity, the LAM¹ phase has the CACB lamellar sequence, whereas the LAM² structure has the BABC layers.

polygons. While the unit cell of $[8.8.4]^2$ contains one 4-coordinated B-domain, 8-coordinated and 4-coordinated microdomains formed by blocks A and C, respectively. From the phase path, in tiling patterns, the coordination number of C-domains is proportional to the volume fraction of f_C . With the increment of f_C from 0.18 to 0.50, the coordinations of C-domains change from 4, to 6, to 8, then to 10 (in the $[3.3.4.3.4]$ phase), finally to 12. Further increasing f_C , the asymmetry of A (B) arm and C arm results in arrangement of junctions on a curve line. Then a 3D structure of TPL appears when $0.51 \leq f_C \leq 0.58$. When $f_C > 0.58$, the lamellar phase LAM^2 is stable in which the

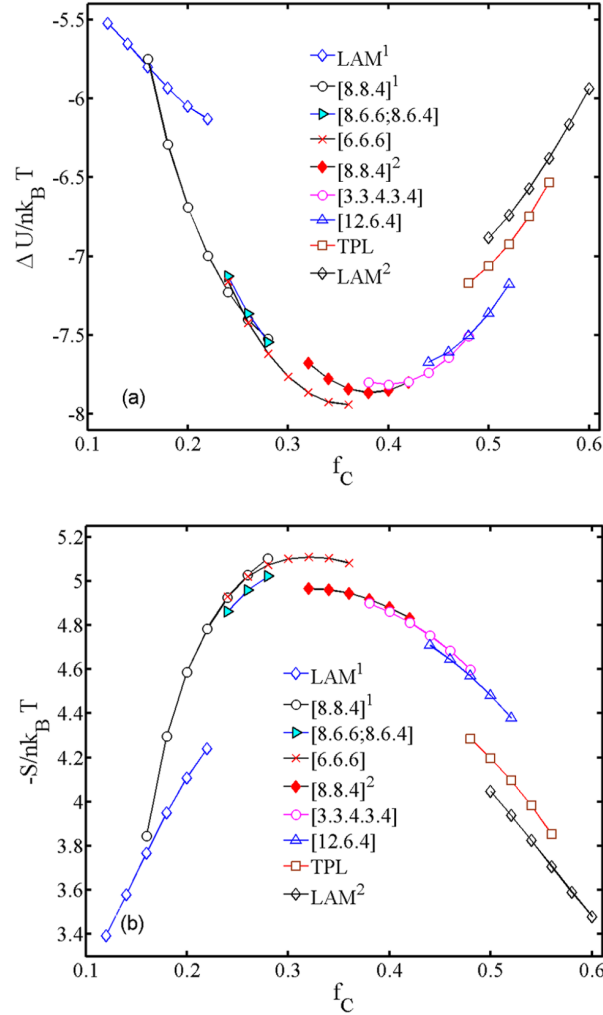


Figure 3: (a) Internal energy of $\Delta U/nk_B T$ and (b) entropic energy of $-S/nk_B T$ of various structures as a function of f_C on the phase path of $f_A = f_B$. The morphologies of $[8.8.4]^1$, $[8.8.4]^2$, LAM^1 and LAM^2 are explained in Fig. 2.

arrangement manner is BABC type in one period, including one thick C layer and three thin BAB

layers.

We can analyze the stability of these ordered phases after splitting the SCFT energy functional into the internal and entropic parts (see Eq. (??)). Fig. 3 gives the internal energy $\Delta U/nk_B T$, subtracted by that of the homogeneous phase,²⁵ together with the entropic energy of $-S/nk_B$, as a function of f_C . From Fig. 3 (a), we can find that LAM¹ (CACB layers) has very high internal energy at small f_C which is induced by the penetrations of A and B arms through C domains.²⁵ At the same time, the lamellae of LAM¹ is favorable from the aspect of entropic energy, because the A and B blocks can get the largest entropy in the lamellar structure when they have equal large lengths compared with the C blocks. The combination of the two contributions makes the LAM¹ be the stable phase when $f_C \leq 0.18$. When increasing f_C , the internal energy becomes dominant and the stable phase transfers from LAM¹ to the cylindrical structures where the arm penetrations in dissimilar phase regions are diminished. When the stable phase transfers from [8.8.4]² to [3.3.4.3.4] (also termed as [10.8.4; 10.6.4]), the entropic energy plays a dominant role on the stability. It is attributed to the increment of C arm which tends to form large C-domains. The enlarged C-domains have an opportunity to meet much more A-domains which will increase the internal energy due to the largest interaction parameter $\chi_{AC}N$. On the other hand, as the arm C increases, the A and B arms become shorter. The A and B arms can freely stretch in their rich domains which can greatly reduce the entropic energy. The explanation is also available to the appearance of [12.6.4], TPL as stable phases. Further increasing f_C to 0.58, the lamellar phase of LAM² (BABC layers) is stable again. The reason is similar to that of the stability of LAM¹ phase when f_C is smaller than 0.18.

Along this phase path, Matsushita and co-workers¹³ synthesized a set of I_{1.0}S_{1.0}P_x copolymers and observed a number of ordered structures. Four ISP star triblock copolymers with volume ratios of 1.0:1.0:0.7, 1.0:1.0:1.2, 1.0:1.0:1.3, and 1.0:1.0:1.9 were investigated. The cylindrical structures of I_{1.0}S_{1.0}P_{0.7}, I_{1.0}S_{1.0}P_{1.2}, I_{1.0}S_{1.0}P_{1.3}, and I_{1.0}S_{1.0}P_{1.9} are [6.6.6], [8.8.4], [3.3.4.3.4], and [12.6.4], respectively. From our simulations, the resulting phase behavior is in good agreement with these experimental measurements when $0.7 < x < 2.0$. At higher asymmetries, Takano et al.⁴⁶ observed

an L+S phase in $I_{1.0}S_{1.0}P_{0.2}$ system, and an L+C phase in $I_{1.0}S_{1.0}P_{3.0}$ and $I_{1.0}S_{1.0}P_{4.9}$ copolymers. However, in our calculations, the LAM phase dominates the regions. This might be attributed to the relatively weak interaction parameters of $\chi_{AB}N$ or $\chi_{BC}N$ in our simulations so that a further segregation between components A and B (or B and C) can not occur. In 2007, Hayashida et al.¹⁵ have discovered a cylinders-in-lamella phase in which the stacking manner of the cylinders seems to be random in the experiments of ISP star triblock copolymer melts. In our calculations, the cylinders-in-lamella, TPL, is found to be stable when $0.51 \leq f_C \leq 0.56$, in which the cylinders are stacking tetragonally. The discrepancy is attributed to the thermodynamic fluctuations which may affect the arrangement of cylinders under experimental circumstances. While within the mean-field level theory, the fluctuations have been neglected.

Along the similar phase path, Nunns et al.¹⁷ synthesized a set of ISF star triblock copolymers and observed the polygonal tilings [8.8.4] and [12.6.4]. Our resulting phase behavior is generally consistent with the ISF experiments. A deviation between our theoretical results and experiments is that the [12.6.4] was observed in $I_{0.40}S_{0.37}F_{0.23}$ system. The discrepancy can be attributed to the different interactions, and different monomer sizes.

Our computational results also agree with the previous theoretical calculations.^{21,24,25} Among these works, Zhang et al.²⁴ considered 2D tiling patterns and chose the asymmetric Flory-Huggins interaction parameters of $\chi_{AC}N = 37.0$, $\chi_{AB}N = \chi_{BC}N = 25.0$ to model the system of ABC star triblock copolymers. A 1D phase diagram of the star triblock copolymers $A_{1.0}B_{1.0}C_x$ was obtained. With the increase of x , the phase transition changes from $[8.8.4]^1$ to $[8.8.4]^2$, then to $[8.6.6;8.6.4]$ and finally to [12.6.4]. The corresponding stable regions are $0.50 \leq x \leq 0.86$, $0.94 \leq x \leq 1.33$, $x \approx 1.45$ and $1.57 \leq x \leq 2.00$, respectively. The phase behaviors of $[8.8.4]^1$, $[8.8.4]^2$, and [12.6.4] are qualitatively consistent with our results. There are some discrepancies between their results and our computer simulations. In their phase diagram, the Archimedean tiling of [3.3.4.3.4] is not included in their simulations, the order pattern [6.6.6] is metastable, and the stable area of $[8.6.6;8.6.4]$ is different from ours. The discrepancies can be attributed to two aspects. The first one is that more candidate structures are involved in our simulations. The second one is the difference

of the Flory-Huggins interaction parameters.

Phase Behavior of $A_{1.0}B_xC_{1.0}$ Star Triblock Copolymers

On the above phase path, many candidate structures, such as 2D polygonal phases [10.6.6;10.6.4; 8.6.6;8.6.4] and 3D hierarchical structures of HHC, HDG, do not appear. To obtain the stability regions of the 2D and 3D phases which have been observed in experiments, we turn to another phase path of isopleth $f_A = f_C$, i.e., by fixed equal length of arms A and C and the arm-length ratio of $1.0 : x : 1.0$ with an increment of volume fraction f_B of 0.01. The free energy difference from the value of the homogeneous phase as a function of f_B varying from 0.20 to 0.68 is plotted in Fig. 4 (a). The phase stability regions as a function of x are presented in Fig. 4 (b). Along this phase path, the phase sequence with increasing f_B is LAM \rightarrow [8.8.4] \rightarrow [6.6.6] \rightarrow [10.6.6;10.6.4;8.6.6;8.6.4] \rightarrow L+C \rightarrow HDG \rightarrow HHC \rightarrow [12.6.4].

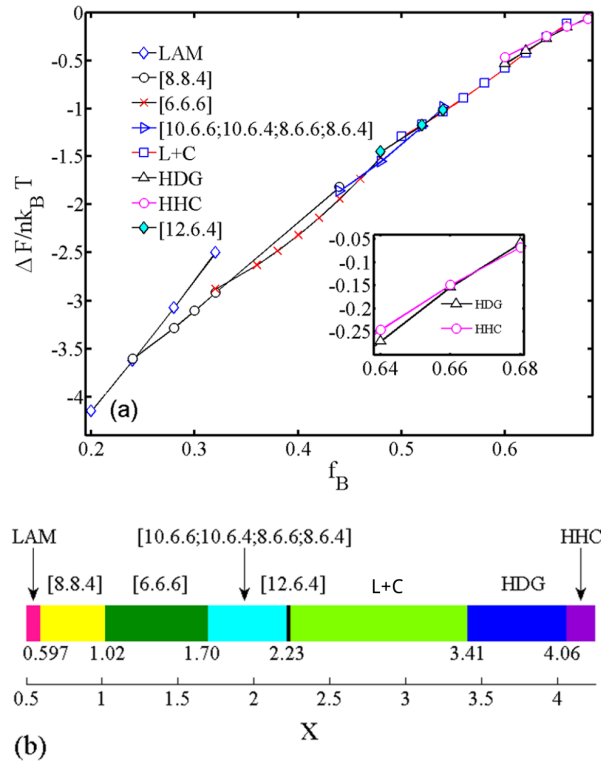


Figure 4: (a) The free energy differences of various candidate phases, from the value of the homogeneous phase, as a function of f_B for ABC star triblock copolymers with symmetric A and C arms. (b) Phase stability regions as a function of the arm-length ratio of $x = f_B/f_A$ ($f_A = f_C$) of ABC star triblock copolymers with asymmetric interactions, $\chi_{AC}N = 50.0$, $\chi_{AB}N = \chi_{BC}N = 30.0$ as a function of the arm-length ratio of $x = f_B/f_A$.

[10.6.6;10.6.4;8.6.6;8.6.4] \rightarrow [12.6.4] \rightarrow L+C \rightarrow HDG \rightarrow HHC. The stable region of LAM phase is $f_B \leq 0.24$. At the center part of the phase path, the chain lengths of three arms are close to one another, junction points are aligned on a straight line, and hence 2D tiling patterns can be formed. The stability regions of 2D cylindrical phases are $0.24 \leq f_B \leq 0.33$ ([8.8.4]), $0.33 \leq f_B \leq 0.46$ ([6.6.6]), $0.46 \leq f_B \leq 0.52$ ([10.6.6;10.6.4;8.6.6;8.6.4]), $f_B \approx 0.53$ ([12.6.4]), respectively. From the phase path, we can also find that, in polygonal patterns, the coordinations of B-domains are proportional to the volume fraction of f_B . With the increase of f_B from 0.24 to 0.53, the coordination number of B-domains goes through a gradual change from 4 ([8.8.4]¹), 6 ([6.6.6]), 8 or 10 ([10.6.6;10.6.4;8.6.6;8.6.4] tiling), to 12 ([12.6.4]).

Further increasing f_B , the A and C arms become shorter. Also, owing to the largest interaction parameter $\chi_{AC}N$, a further segregation between two minority blocks A and C occurs within the large-length-scale phase, and the system can form some hierarchical morphologies. The interesting hierarchical patterns include 2D L+C phase, and 3D patterns of HDG, HHC, and their stability regions are $0.54 \leq f_B \leq 0.63$ (L+C), $0.63 \leq f_B \leq 0.67$ (HDG), $f_B \geq 0.67$ (HHC), respectively.

After splitting the SCFT energy functional into internal energy and entropic energy as expressed in Eqn. (??) (see Fig. 5), the stability of 3D hierarchical structures HHC and HDG along the phase path can be understood more readily. When the ratio of $x = f_B/f_A$ ($f_A = f_C$) is large enough, the asymmetric ABC star triblock copolymers will exhibit similar phase behavior of asymmetric diblock copolymer. The longest B arm plays an equal role as the long block in an asymmetric diblock copolymer, whereas the short A arm, together with C arm, are just like the short block in the diblock copolymer. In asymmetric diblock copolymers, the systems tend to curve the interface towards the minority domain. It requires the minority block to stretch, and the cost is more than compensated for by relaxation of the longer blocks, which increases the internal energies.²⁸ Besides the asymmetry of blocks, the segregation power between arms A and C, $\chi_{AC}N$, is sufficiently large to separate the A-, and C-domains, leading to the formation of hierarchical structures. In particular, for the asymmetric ABC star copolymers, the blocks A and C have shorter chains than the short block in AB diblock when the curve interface can be formed. The A and C arms can

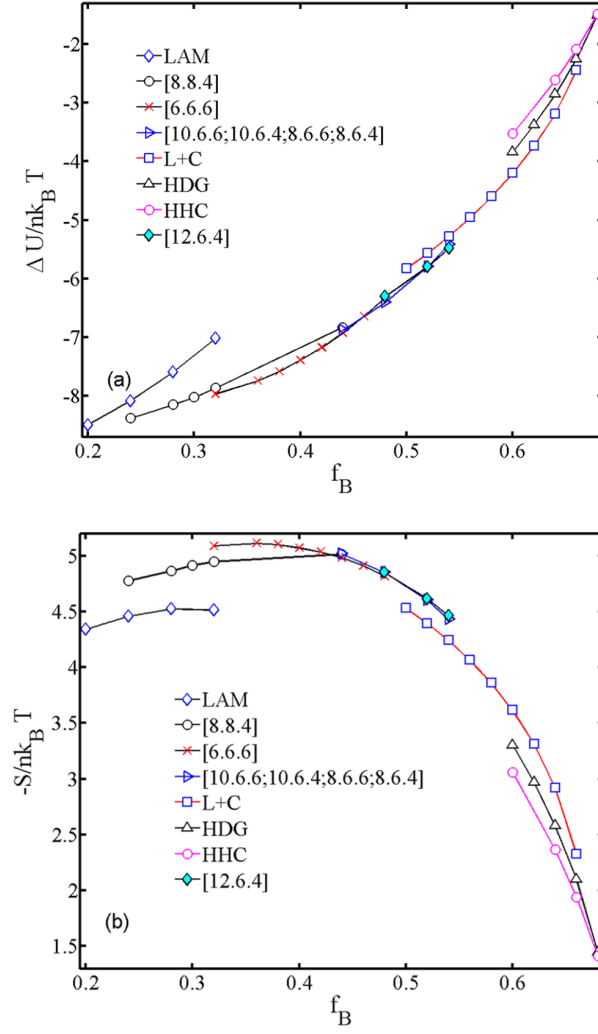


Figure 5: (a) Internal energy of $\Delta U / nk_B T$ and (b) entropic energy of $-S / nk_B T$ of various structures as a function of f_B on the phase path of $f_A = f_C$.

freely relax in their packing frustration domains which greatly reduces the entropic energy of the system. Although the internal energies of 3D hierarchical structures are higher than that of L+C structure, their entropic energies are much lower than that of the 2D cylinders-in-lamella phase. As a consequence, the combination of the two competing energies makes 3D hierarchical structures stable rather than L+C when $f_B \geq 0.63$. At higher asymmetries, block copolymers prefer to form structures with a higher interfacial curvature.⁴⁷ Therefore HHC phase with larger spontaneous curvature than that of HDG phase, has lower free energy when $f_B \geq 0.67$.

Triangular Phase Diagram

The phase transition sequence for systematically varying volume fractions can be obtained by repeating the free energy comparison among the candidate structures. The results of the phase transition sequences can be summarized in terms of phase diagrams. For the case of asymmetric interaction parameters of $\chi_{AC}N > \chi_{AB}N = \chi_{BC}N$, the triangular phase diagram is mirror symmetric with the axes of $f_A = f_C$. Therefore one-half of the whole triangular phase diagram should be calculated. The triangular phase diagram obtained by our SCFT simulations is presented in Fig. 6. Sixteen structures, including 2D, 3D ordered phases and disordered phase (D), are predicted to be stable in the phase diagram. Besides the [6.6.6], [8.8.4], [8.6.6; 8.6.4], [3.3.4.3.4], [10.6.6;10.6.4;8.6.6;8.6.4], [12.6.4], L+C, TPL, HHC, HDG and LAM phases discussed above, four more ordered structures, HPL, core-shell structures of HC, DG, and BCC, and disordered phase are included in the triangular phase diagram. The regions of stability of the different phases are obtained by comparing the free energy of these candidate structures. The phase boundaries are determined by calculating the cross over point of the free energies of the two neighbouring phases. The most significant feature of the triangular phase diagram is the rich phase behavior with a large number of stable ordered phases. It should be noted that the ordered structures emerging in diblock copolymers, i.e., no core-shell cylinders, spheres, gyroid, two-color lamella, are not included in our calculations. That is, near the boundary of the triangular phase diagram, simulations are not carried out in our study.

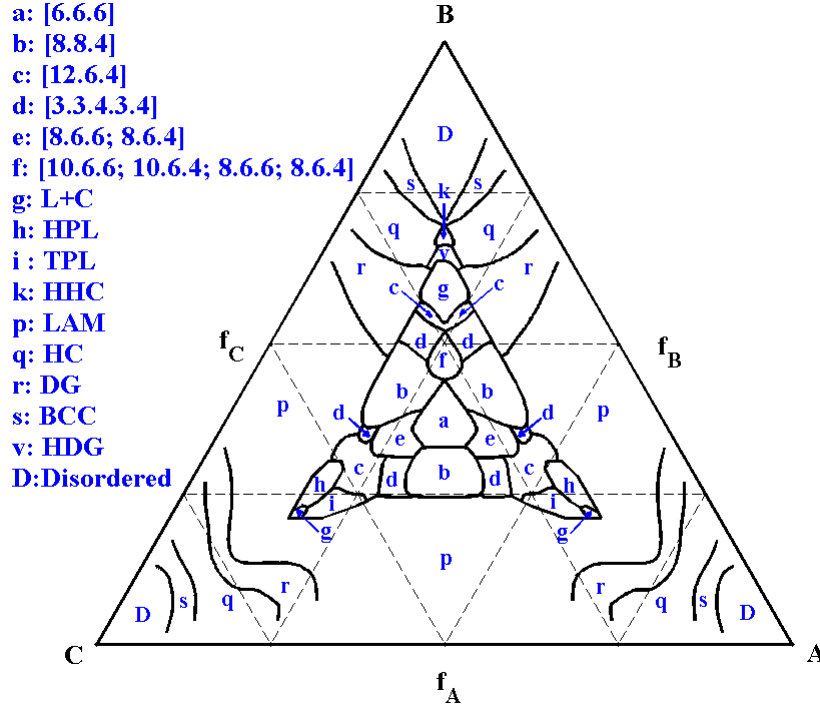


Figure 6: The triangular phase diagram of ABC star triblock copolymers with equal statistical segment lengths for each block and with asymmetric interaction parameters of $\chi_{AC}N = 50.0$, $\chi_{AB}N = \chi_{BC}N = 30.0$. The ordered structures emerging in diblock copolymers, i.e., no core-shell cylinders, spheres, gyroid, two-color lamella, are not included in our calculations. That is, near the boundary of the triangular phase diagram, simulations are not carried out in our study.

When the chain lengths of three arms are close to each other, junction points are aligned on a straight line, and hence the system tends to form polygonal tilings to get smaller internal energy. As a consequence, the central region of the phase map is dominated by the 2D tiling patterns. The coordination number of each domain is proportional to the composition of corresponding block. For example, as discussed above, along the phase path of $f_A : f_B : f_C = 1.0 : 1.0 : x$, the coordination number of C-domains changes from 4, to 6, to 8, then to 10, and finally to 12 with increasing of x from 0.435 to 2.76. Besides the cylindrical structures observed by experiments, two tilings of [8.6.6; 8.6.4] and [10.6.6;10.6.4;8.6.6;8.6.4] are predicted as the stable phases in our theoretical calculations. The stability has been analyzed in the above context. It is very different from the phase behavior of ABC linear triblock copolymer melt in which the lamellar phase occupies the large central region.⁴⁸ The reason is attributed to the topology of the star copolymer chain for which the junction points tend to be aligned on a straight line when the chain lengths of three arms are comparable. As the compositions of star copolymer become asymmetric, more 2D and 3D phases, including LAM, HC, DG, BCC, HPL, TPL and cylinders-in-lamella of L+C, appear and surround these 2D tilings in the triangular phase diagram. Among these phases, LAM phase has the following phase transitions. Near the AB edge, CACB layers can be formed whereas ABAC layers formed near the BC edge, and BABC layers formed near the AC edge.

Consider the structural evolution that starts from the central 2D tilings region, toward the A- and C-rich corners of the triangular phase diagram. The phase transition sequence is the cylinders-in-lamella structures (including HPL and TPL), L+C, LAM, DG, HC, BCC and disordered phase. Near the A-rich corner, in the cylinders-in-lamellar structure, the C arms form internal cylinders in the B perforated lamellar, then blocks B and C form lamellar together with A-layers. The packed manners of the cylinders determine the morphologies of HPL and TPL, as shown in Fig. 1. The 2D hierarchical pattern, L+C, where arms B and C form alternating cylinders in the lamellar-based phase, has a stable region between cylinders-in-lamellar structures and LAM phase. The prediction of stability region of L+C phase is generally consistent with the recent experiment in which Nunns et al. observed the phase in $I_{0.20}S_{0.14}F_{0.66}$ star copolymer system.¹⁷ Because of the smallness of

χ_{BC} , a further segregation between the minority components B and C (A and B) will not occur, which implies that the 3D hierarchical structures will not be global stable in this region. Instead, the LAM phase dominates this area. Owing to $\chi_{BC} = \chi_{AB}$, there is similar phase behavior near the C-rich corner when exchanging the position of arms A and C.

The BCC, HC, and DG phases form continuous areas across the A- and C-rich corners of the triangular phase diagram, where A or C block is the largest arm. The continuous areas formed by these phases in the triangular phase diagram reflect a continuous evolution in the compositions of the core and shell blocks. For example, consider the evolution of structure along a path within the BCC phase in the A-rich corner, starting from the AB edge, where the structure contains B spheres in an A matrix, to the AC edge. As the C arm increases its length, a spherical “shell” of C grows in the middle of each B-sphere, while the composition of the surrounding shell of B shrinks, until a structure of C spheres in an A matrix is obtained at the AC edge. An analogous change in the volume fractions of the “shell” and “core” components occurs in the HC and DG phases in both the A- and C-rich corners.

The phase behavior in the B-rich corner is more complicated. Owing to the largest value of $\chi_{AC}N$, the minority components A and C tend to a further segregation near the B-rich corner, which leads to the formation of the hierarchical structures. From the cylindrical regions to B-rich corner, the phase sequence of hierarchical morphologies is $L+C \rightarrow \text{HDG} \rightarrow \text{HHC}$. Near the $f_A = f_C$ line, the stable regions of HC and DG are separated by hierarchical structures of HHC, HDG, L+C and three Archimedean tilings of [12.6.4], [3.3.4.3.4], [8.8.4]. The stable region of BCC phase in the B-rich corner is continuous above that of HHC structure. Consider the structural evolution along a path that starts from the AB edge, where the length of arms satisfies the relationship $f_B > f_A > f_C$, toward the $f_A = f_C$ isopleth. Along this path, for example, in the BCC phase, A arms segregate into spherical domains, surrounded by C-rich pockets shell within the B matrix. The core-shell HC and DG phases have similar phase behavior with A-core, C-shell and B-matrix. Similarly, structures, such as DG, HC, and BCC, evaluating along a path that starts from BC edge toward the $f_A = f_C$ isopleth, are of the C-core, A-shell and B-matrix patterns. In addition, the disordered

phase emerges in the B-rich corner of the triangular phase diagram.

In general, the theoretical phase behavior is in agreement with the experimental observations. However, there are some discrepancies between our theoretical computations and experimental observations. Some structures observed by experiments in ISP star triblock copolymers, such as L+S phase,⁴⁶ Zinc-blende type structure⁶ are not obtained in our simulations. The stable regions of some structures obtained by experiments are not exactly located in the predicted phase regions of our phase diagram. Our theoretical phase diagram predicted [8.6.6; 8.6.4] and [10.6.6;10.6.4;8.6.6;8.6.4] as stable phases which have been not observed in the experiments. There are three main possible reasons for these discrepancies. The first one is that in the experiments many star triblock copolymers are obtained by blending two kinds of copolymers, or adding additional homopolymers. For example, the Zinc-blende type structure was observed in the $I_{1.0}S_{2.3}P_{0.8}$ system which was realized by blending the S homopolymer to $I_{1.0}S_{1.8}P_{0.8}$. The homopolymer S can definitely affect the phase stabilities. The second one is that the predicted phases in the theoretical calculation, such as the [8.6.6;8.6.4] and [10.6.6;10.6.4;8.6.6;8.6.4], may be metastable in the recent experimental systems. The third one is that there are many differences between theoretical systems and experimental conditions, such as the different interactions, different monomer sizes. In our calculations, we neglect the differences between $\chi_{AB}N$ and $\chi_{BC}N$. The difference is small, however, it might influence the self-assembling behavior. At the same time, the values of interaction may be different from the experimental systems.

Conclusions

In this work, we have investigated the phase behavior of ABC star triblock copolymers with asymmetric interaction parameters using the SCFT. Based on the previous work of screening initialization strategies,²⁷ we can obtain a large number of ordered phases in studying the complex polymer systems. Then we used a fourth-order pseudospectral method, combined with the Anderson mixing algorithm to calculate the free energy of the observed phases. Motivated by previously experimen-

tal studies, the Flory-Huggins interaction parameters of $\chi_{BC}N = \chi_{AB}N = 30.0$, $\chi_{AC}N = 50.0$ are used to model the experimental systems of ISP and ISF star copolymers in bulk. To extend the scope of theoretical study, a large number of 2D and 3D ordered structures have been involved in our calculations. In order to shed light on the phase behavior of the ABC star triblock copolymers, we first determined the phase stability along the phase path $f_A : f_B : f_C = 1.0 : 1.0 : x$. Our results agree with those of ISP star triblock copolymers for cylindrical phases well. Then we calculated the phase regions along the phase path $f_A : f_B : f_C = 1.0 : x : 1.0$. On this phase path, besides the cylindrical structures, we emphatically analyzed the stability of hierarchical structures of L+C, HDG, HHC. The phase stability has been analyzed by splitting the SCFT energy functional into internal and entropic parts in detail. Finally we constructed a very complicated triangular phase diagram with these candidate structures. Owing to the case of interactions $\chi_{BC}N = \chi_{AB}N$, the phase diagram has only one mirror symmetric axis $f_A = f_C$. Fifteen ordered structures and the inhomogeneous phase constitute the triangular phase diagram. In general, the phase regions predicted by our SCFT calculations are consistent with previous theoretical studies of either SCFT calculations or MC, DPD simulations which mainly focus on the equal interaction systems. However, in our calculations, the interaction parameters are more closely related to experimental systems, such as ISP and ISF star triblock copolymers, i.e., the asymmetric interaction parameters $\chi_{AC}N > \chi_{BC}N = \chi_{AB}N$. It has been found that the asymmetry of the interaction parameters plays a profound role in the complex phase formation. Furthermore, our predicted phase diagram involves more phases, especially 3D structures, and presents more comprehensive phase behavior. Our calculations and analysis can be helpful to understand the self-assembling mechanism of complex structures. The resulting phase behavior extends the theoretical study to the asymmetrically interacting ABC star triblock copolymers. And the presented phase diagram will be a useful guide for further study of ABC star triblock copolymers.

References

- (1) Bates, F. S.; Hillmyer, M. A.; Lodge, T. P.; Bates, C. M.; Delaney, K. T.; Fredrickson, G. H. Multiblock Polymers: Panacea or Pandora's Box ? *Science* **2012**, 336, 434-440.
- (2) Hamley, I. W. *Developments in Block Copolymer Science and Technology*, Wiley; New York, 2004.
- (3) Park, C.; Yoon, J.; Thomas, E. L. Enabling Nanotechnology with Self Assembled Block Copolymer Patterns. *Polymer* **2003**, 44, 6725-6760.
- (4) Meng, F.; Zhong, Z.; Feijen, J. Stimuli-Responsive Polymersomes for Programmed Drug Delivery. *Biomacromolecules* **2009**, 10, 197-209.
- (5) Ruiz, R.; Kang, H.; Detcheverry, F. A.; Dobisz, E.; Kercher, D. S.; Albrecht, T. R.; de Pablo, J. J.; Nealey, P. F. Density Multiplication and Improved Lithography by Directed Block Copolymer Assembly. *Science* **2008**, 321, 936-939.
- (6) Matsushita, Y.; Hayashida, K.; Takano, A. Jewelry Box of Morphologies with Mesoscopic Length Scales—ABC Star-shaped Terpolymers. *Macromol. Rapid Commun.* **2010**, 31, 1579-1587.
- (7) Matsushita, Y.; Hayashida, K.; Dotera, T.; Takano, A. Kaleidoscopic Morphologies from ABC Star-Shaped Terpolymers. *J. Phys.: Condens. Matter* **2011**, 23, 284111.
- (8) Okamoto, S.; Hasegawa, H.; Hashimoto, T.; Fujimoto, T.; Zhang, H.; Kazama, T.; Takano, A.; Isono, Y. Morphology of Model Three-Component Three-Arm Star-Shaped Copolymers. *Polymer* **1997**, 38, 5275-5281.
- (9) Sioula, S.; Hadjichristidis, N.; Thomas, E. L. Direct Evidence for Confinement of Junctions to Lines in an 3 Miktoarm Star Terpolymer Microdomain Structure. *Macromolecules* **1998**, 31, 8429-8432.

- (10) Sioula, S.; Hadjichristidis, N.; Thomas, E. L. Novel 2-Dimensionally Periodic Non-Constant Mean Curvature Morphologies of 3-Miktoarm Star Terpolymers of Styrene, Isoprene, and Methyl Methacrylate. *Macromolecules* **1998**, 31, 5272-5277.
- (11) Takano, A.; Wada, S.; Sato, S.; Araki, T.; Hirahara, K.; Kazama, T.; Kawahara, S.; Isono, Y.; Ohno, A.; Tanaka, N.; Matsushita, Y. Observation of Cylinder-Based Microphase-Separated Structures from ABC Star-Shaped Terpolymers Investigated by Electron Computerized Tomography. *Macromolecules* **2004**, 37, 9941-9946.
- (12) Takano, A.; Kawashima, W.; Noro, A.; Isono, Y.; Tanaka, N.; Dotera, T.; Matsushita, Y. A Mesoscopic Archimedean Tiling Having a New Complexity in an ABC Star Polymer. *J. Polym. Sci. Part B: Polym. Phys.* **2005**, 43, 2427-2432.
- (13) Hayashida, K.; Kawashima, W.; Takano, A.; Shinohara, Y.; Amemiya, Y.; Nozue, Y.; Matsushita, Y. Archimedean Tiling Patterns of ABC Star-Shaped Terpolymers Studied by Microbeam Small-Angle X-ray Scattering. *Macromolecules* **2006**, 39, 4869-4872.
- (14) Matsushita, Y. Creation of Hierarchically Ordered Nanophase Structures in Block Polymers Having Various Competing Interactions. *Macromolecules* **2007**, 40, 771-776.
- (15) Hayashida, K.; Saito, N.; Arai, S.; Takano, A.; Tanaka, N.; Matsushita, Y. Hierarchical Morphologies Formed by ABC Star-Shaped Terpolymers. *Macromolecules* **2007**, 40, 3695-3699.
- (16) Hückstädt, H.; Göpfert, A.; Abetz, V. Synthesis and Morphology of ABC Heteroarm Star Terpolymers of Polystyrene, Polybutadiene and Poly(2-vinylpyridine). *Macromol. Chem. Phys.* **2000**, 201, 296-307.
- (17) Nunns, A.; Ross, C. A.; Manners, I. Synthesis and Bulk Self-Assembly of ABC Star Terpolymers with a Polyferrocenylsilane Metalloblock. *Macromolecules* **2013**, 46, 2628-2635.
- (18) Park, J.; Jang, S.; Kim, J. K. Morphology and Microphase Separation of Star Copolymers. *J. Polym. Sci. Part B: Polym. Phys.* **2015**, 53, 1-21.

- (19) Hayashida, K.; Dotera, T.; Takano, A.; Matsushita, Y. Polymeric Quasicrystal: Mesoscopic Quasicrystalline Tiling in ABC Star Polymers. *Phys. Rev. Lett.* **2007**, 98, 195502.
- (20) Bohbot-Raviv, Y.; Wang, Z.-G. Discovering New Ordered Phases of Block Copolymers. *Phys. Rev. Lett.* **2000**, 85, 3428-3431.
- (21) Gemma, T.; Hatano, A.; Dotera, T. Monte Carlo Simulations of the Morphology of ABC Star Polymers Using the Diagonal Bond Method. *Macromolecules* **2000**, 35, 3225-3237.
- (22) Huang, C. I.; Fang, H. K.; Lin, C. H. Morphological Transition Behavior of ABC Star Copolymers by Varying the Interaction Parameters. *Phys. Rev. E* **2008**, 77, 031804.
- (23) Tang, P.; Qiu, F.; Zhang, H.; Yang, Y. Morphology and Phase Diagram of Complex Block Copolymers: ABC Star Triblock Copolymers. *J. Phys. Chem. B* **2004**, 108, 8434-8428.
- (24) Zhang, G.; Qiu, F.; Zhang, H.; Yang, Y.; Shi, A.-C. SCFT Study of Tiling Patterns in ABC Star Terpolymers. *Macromolecules* **2010**, 43, 2981-2989.
- (25) Li, W.; Xu, Y.; Zhang, G.; Qiu, F.; Yang, Y.; Shi, A.-C. Real-Space Self-Consistent Mean-Field Theory Study of ABC Star Triblock Copolymers. *J. Chem. Phys.* **2010**, 133, 064904.
- (26) Xu, Y.; Li, W.; Qiu, F.; Zhang, H.; Yang, Y.; Shi, A.-C. Stability of Hierarchical Lamellar Morphologies Formed in ABC Star Triblock Copolymers. *J. Polym. Sci. Part B: Polym. Phys.* **2010**, 48, 1101-1109.
- (27) Xu, W.; Jiang, K.; Zhang, P.; Shi, A.-C. A Strategy to Explore Stable and Metastable Ordered Phases of Block Copolymers. *J. Phys. Chem. B* **2013**, 117, 5296-5305.
- (28) Matsen, M. W. The Standard Gaussian Model for Block Copolymer Melts. *J. Phys.: Condens. Matter* **2002**, 14, R21-R47.
- (29) Fredrickson, G. H. *The Equilibrium Theory of Inhomogeneous Polymers*; Oxford University Press: New York, 2006.

- (30) Jiang, K.; Huang, Y.; Zhang, P. Spectral Method for Exploring Patterns of Diblock Copolymers. *J. Comput. Phys.* **2000**, 229, 7796-7805.
- (31) Jiang, K.; Wang, C.; Huang, Y.; Zhang, P. Discovery of New Metastable Patterns in Diblock Copolymers. *Commun. Comput. Phys.* **2013**, 14, 443-460.
- (32) Matsen, M. W.; Schick, M. Stable and Unstable Phases of a Diblock Copolymer Melt. *Phys. Rev. Lett.* **1994**, 72, 2660-2663.
- (33) Guo, Z.; Zhang, G.; Qiu, F.; Zhang, H.; Yang, Y.; Shi, A.-C. Discovering Ordered Phases of Block Copolymers: New Results from a Generic Fourier-Space Approach. *Phys. Rev. Lett.* **2008**, 101, 28301.
- (34) Drolet, F.; Fredrickson, G. H. Combinatorial Screening of Complex Block Copolymer Assembly with Self-Consistent Field Theory. *Phys. Rev. Lett.* **1999**, 83, 4317-4320.
- (35) Rasmussen, K. Ø.; Kalosakas, G. Improved Numerical Algorithm for Exploring Block Copolymer Mesophases. *J. Phys.: Condens. Matter* **2002**, 40, 1777-1783.
- (36) Cochran, E. W.; Garcia-Cervera, C. J.; Fredrickson, G. H. Stability of the Gyroid Phase in Diblock Copolymers at Strong Segregation. *Macromolecules* **2006**, 39, 2449-2451.
- (37) Ranjan, A.; Qin, J.; Morse, D. C. Linear Response and Stability of Ordered Phases of Block Copolymer Melts. *Macromolecules* **2008**, 41, 942-954.
- (38) Cenicerros, H. D.; Fredrickson, G. H. Numerical Solution of Polymer Self-Consistent Field Theory. *Multiscale Model. Simul.* **2004**, 2, 452-474.
- (39) Jiang, K.; Xu, W.; Zhang P. Analytic Structure of the SCFT Energy Functional of Multicomponent Block Copolymers. *Commun. Comput. Phys.* **2015**, 17, 1360-1387.
- (40) Schmid, F.; Müller M. Quantitative Comparison of Self-Consistent Field Theories for Polymers near Interfaces with Monte Carlo Simulations. *Macromolecules* **1995**, 28, 8639-8645.

- (41) Thompson R. B.; Rasmussen K. Ø.; Lookman T. Improved Convergence in Block Copolymer Self-Consistent Field Theory by Anderson Mixing. *J. Chem. Phys.* **2004**, 120, 31-34.
- (42) See the formula (4.1.14) on p. 160 in *Numerical Recipes: The Art of Scientific Computing*, 3rd edition, Press, W. H.; Teukolsky, S. A.; Vetterling, W. T.; Flannery, B. P., Ed.; Cambridge University Press; New York, 2007.
- (43) Anderson, D. G. Iterative Procedures for Nonlinear Integral Equations. *J. ACM* **1965**, 12, 547-560.
- (44) Matsen, M. W. Fast and Accurate SCFT Calculations for Periodic Block-Copolymer Morphologies using the Spectral Method with Anderson Mixing. *Eur. Phys. J. E* **2009**, 30, 361-369.
- (45) V. Abetz, Block Copolymers, Ternary Triblocks, in: *Encyclopedia of Polymer Science and Technology*, 3rd edition, Kroschwitz, J. I. Ed.; John Wiley & Sons, Inc, Vol. 1, 2003.
- (46) Takano A.; Kawashima W.; Wada S.; Hayashida K.; Sato S.; Kawahara S.; Isono Y.; Maki-hara M.; Tanaka N.; Kawaguchi D.; Matsushita Y. Composition Dependence of Nanophase-Separated Structures Formed by Star-Shaped Terpolymers of the $A_{1.0}B_{1.0}C_X$ Type. *J. Polym. Sci. Part B: Polym. Phys.* **2007**, 45, 2277-2283.
- (47) Matsen, M. W.; Bates, F. S. Origins of Complex Self-Assembly in Block Copolymers. *Macromolecules* **1996**, 29, 7641-7644.
- (48) Tyler, C. A.; Qin, J.; Bates, F. S.; Morse, D. C. SCFT Study of Nonfrustrated ABC Triblock Copolymer Melts. *Macromolecules* **2007**, 40, 4654-4668.

Appendix: The Implementation of Anderson Mixing Method

The k iteration in the Anderson mixing method begins with the evaluation of new fields from Eqns. (??)-(??)

$$\eta^{(k)}(\mathbf{r}) = \frac{\sum_{\alpha=A,B,C} w_{\alpha}^{(k)}(\mathbf{r}) X_{\alpha} - 2N\chi_{AB}\chi_{BC}\chi_{AC}}{\sum_{\alpha} X_{\alpha}}, \quad (12)$$

$$\bar{w}_A^{(k)}(\mathbf{r}) = \chi_{AB}N\phi_B^{(k)}(\mathbf{r}) + \chi_{AC}N\phi_C^{(k)}(\mathbf{r}) + \eta(\mathbf{r}), \quad (13)$$

$$\bar{w}_B^{(k)}(\mathbf{r}) = \chi_{AB}N\phi_A^{(k)}(\mathbf{r}) + \chi_{BC}N\phi_C^{(k)}(\mathbf{r}) + \eta(\mathbf{r}), \quad (14)$$

$$\bar{w}_C^{(k)}(\mathbf{r}) = \chi_{AC}N\phi_A^{(k)}(\mathbf{r}) + \chi_{BC}N\phi_B^{(k)}(\mathbf{r}) + \eta(\mathbf{r}). \quad (15)$$

In the above expressions, $w_{\alpha}^{(k)}$, $\alpha = A, B, C$, are the old fields, $X_A = \chi_{BC}(\chi_{AB} + \chi_{AC} - \chi_{BC})$, $X_B = \chi_{AC}(\chi_{BC} + \chi_{AB} - \chi_{AC})$, $X_C = \chi_{AB}(\chi_{AC} + \chi_{BC} - \chi_{AB})$. Next we evaluate the deviation,

$$d^{(k)} = \bar{w}^{(k)}(\mathbf{r}) - w^{(k)}(\mathbf{r}), \quad (16)$$

where $d^{(k)} = (d_A^{(k)}(\mathbf{r}), d_B^{(k)}(\mathbf{r}), d_C^{(k)}(\mathbf{r}))^T$, $\bar{w}^{(k)}(\mathbf{r}) = (\bar{w}_A^{(k)}(\mathbf{r}), \bar{w}_B^{(k)}(\mathbf{r}), \bar{w}_C^{(k)}(\mathbf{r}))^T$, $w^{(k)}(\mathbf{r}) = (w_A^{(k)}(\mathbf{r}), w_B^{(k)}(\mathbf{r}), w_C^{(k)}(\mathbf{r}))^T$. From the deviation we can specify an error tolerance through the inner product

$$(g(\mathbf{r}), f(\mathbf{r})) = \frac{1}{V} \int d\mathbf{r} g(\mathbf{r}) f(\mathbf{r}), \quad (17)$$

where $g(\mathbf{r})$ and $f(\mathbf{r})$ are arbitrary functions. The error tolerance is defined by

$$\varepsilon_1 = \left[\frac{\sum_{\alpha=A,B,C} (d_{\alpha}^{(k)}(\mathbf{r}), d_{\alpha}^{(k)}(\mathbf{r}))}{\sum_{\alpha=A,B,C} (w_{\alpha}^{(k)}(\mathbf{r}), w_{\alpha}^{(k)}(\mathbf{r}))} \right]^{1/2} \quad (18)$$

as a measure of the numerical inaccuracy in the field Eqns. (??)-(??).

The simple mixing method is performed until a certain tolerance is reached where a morphology has begun to develop. From our experience, $\varepsilon_1 < 10^{-2}$, is sufficient in most cases. We then switch to the Anderson mixing procedure by the previous n steps to update fields. We assemble

the symmetric matrix in this way

$$U_{ij}^{(k)} = (d^{(k)} - d^{(k-i)}, d^{(k)} - d^{(k-j)}), \quad (19)$$

for $i, j = 1, 2, \dots, n$, and vector

$$V_i^{(k)} = (d^{(k)} - d^{(k-i)}, d^{(k)}) = (d^{(k)}, d^{(k)}) - (d^{(k-i)}, d^{(k)}). \quad (20)$$

From these, we calculate the coefficients

$$C_i = \sum_j^n (U^{-1})_{ij} V_j, \quad (21)$$

and combine the previous histories as

$$T_\alpha^{(k)} = w_\alpha^{(k)} + \sum_{i=1}^n C_i (w_\alpha^{(k-i)} - w_\alpha^{(k)}), \quad (22)$$

$$D_\alpha^{(k)} = d_\alpha^{(k)} + \sum_{i=1}^n C_i (d_\alpha^{(k-i)} - d_\alpha^{(k)}). \quad (23)$$

Finally, the new fields are obtained from

$$w_{\alpha,j}^{(k+1)} = T_{\alpha,j}^{(k)} + \lambda D_{\alpha,j}^{(k)}, \quad (24)$$

where $0 < \lambda = 1.0 - 0.9^k < 1$.⁴⁴

In our implementation, the used previous steps are usually much less than the number of basis functions or grid points. Therefore assembling the n -order linear system spends more computation time than solving this system. To save computational amount, we decompose Eqn. (??) into

$$U_{ij}^{(k)} = (d^{(k)}, d^{(k)}) - (d^{(k-i)}, d^{(k)}) - (d^{(k)}, d^{(k-j)}) + (d^{(k-i)}, d^{(k-j)}). \quad (25)$$

In k iteration, only the terms related to $d^{(k)}$ in the right term of Eqn. (??) are required to calculate,

but the last terms $(d^{(k-i)}, d^{(k-j)})$, $i, j = 1, \dots, n$, should be not computed repeatedly which will save the main computational cost in assembling matrix U . In practical calculations, we store the following inner product matrix

$$S = \begin{pmatrix} (d^{(k)}, d^{(k)}) & (d^{(k)}, d^{(k-1)}) & \dots & (d^{(k)}, d^{(k-n)}) \\ (d^{(k-1)}, d^{(k)}) & (d^{(k-1)}, d^{(k-1)}) & \dots & (d^{(k-1)}, d^{(k-n)}) \\ \vdots & \vdots & \ddots & 0 \\ (d^{(k-n)}, d^{(k)}) & (d^{(k-n)}, d^{(k-1)}) & \dots & (d^{(k-n)}, d^{(k-n)}) \end{pmatrix}. \quad (26)$$

Then we can assemble the matrix U and vector V according to the expressions of Eqns. (??) and (??) using the elements of matrix S . Note that the inner product matrix is symmetric, therefore only a row (or a column, equivalently) of S is required to update in each iteration.